Engineering Applications of Artificial Intelligence 133 (2024) 108044

Contents lists available at ScienceDirect

Engineering Applications of Artificial Intelligence

journal homepage: www.elsevier.com/locate/engappai

Corrosion classification through deep learning of electrochemical noise time-frequency transient information

Axel Homborg [a,b,*], Arjan Mol [b], Tiedo Tinga [a,c]

[a] Netherlands Defence Academy, Faculty of Military Sciences, P.O. Box 10000, 1780CA, Den Helder, The Netherlands
[b] Delft University of Technology, Department of Materials Science and Engineering, Mekelweg 2, 2628CD, Delft, The Netherlands
[c] University of Twente, Faculty of Engineering Technology, P.O. Box 217, 7500AE, Enschede, The Netherlands

ARTICLE INFO

Keywords:
Machine learning
Electrochemical noise transients
Continuous wavelet transform
Modulus maxima
Time-frequency images
Corrosion classification

ABSTRACT

This paper for the first time treats the interpretation of electrochemical noise time-frequency spectra as an image classification problem. It investigates the application of a convolutional neural network (CNN) for deep learning image classification of electrochemical noise time-frequency transient information. Representative slices of these spectra were selected by our transient analysis technique and served as input images for the CNN. Corrosion data from two types of pitting corrosion processes serve as test cases: AISI304 and AA2024-T3 immersed in a 0.01M HCl and 0.1M NaCl solution between 0 and 1ks after immersion, respectively. Continuous wavelet transform (CWT) spectra and modulus maxima (MM) are used to train the CNN, either individually or in a combined form. The classification accuracy of the CNN trained with the combined dataset is 0.97 and with the two individual datasets 0.72 (only CWT spectrum) and 0.84 (only MM). The ability to additionally classify a more progressed form of pitting corrosion of AA2024-T3 between 9 and 10ks after immersion indicates that the proposed method is sufficiently robust using combined datasets with CWT spectra and MM. The pitting processes can effectively be detected and classified by the proposed method. The most important contribution of the present work is to introduce a novel procedure that decreases the classical need for large amounts of raw data for training and validation purposes, while still achieving a satisfactory classification robustness. A relatively small number of individual signals thereby generates a multitude of input images that still contain all relevant kinetic information about the underlying chemo-physical process.

1. Introduction

Electrochemical noise (EN) is a designation used for the spontaneous potential and current variations generated by the charge transfer process during corrosion (Cottis, 2000). The study of EN is used in various fields of corrosion science; examples are the investigation of the corrosion behaviour of aluminium alloys under (semi-) immersed conditions and after different heat treatments (Xia et al., 2023; Rivera-cerezo et al., 2023), of the corrosion inhibition of reinforcement steel in concrete (Recio-Hernández et al., 2023), of stress corrosion cracking and its inhibition (Carmona-Hernandez et al., 2023) and of the corrosion behaviour of dual-phase steels (Montoya-Rangel et al., 2023). EN has the potential to detect general and localized corrosion (Hladky and Dawson, 1981, 1982; Homborg et al., 2014a) and to characterize various aspects of localized corrosion and corrosion inhibition (Denissen et al., 2019; Homborg et al., 2014b, 2022). It however requires the use of effective signal processing tools for this purpose. A very effective class of methods to extract kinetic information about the underlying corrosion process from the EN signal are time-frequency procedures (Aballe et al., 1999a). In selected cases, time-frequency methods have been found to be superior to other data analysis procedures for the characterisation of corrosion (Homborg et al., 2014a). Examples of time-frequency methods are continuous wavelet transform (CWT) and Hilbert-Huang transform (HHT) (Aballe et al., 1999a, 1999b, 2001; Homborg et al., 2013a). CWT and HHT allow the investigation of time-varying frequency components in an EN signal (Aballe et al., 1999a, 1999b, 2001; Homborg et al., 2013a). An example of this is the removal of DC drift from an EN signal, which is of great importance since the DC drift dominates the frequency content of the signal that forms the basis for further analysis. Time-frequency methods have shown the ability to define an exact part of the signal as DC drift (Homborg et al., 2012). Time-frequency methods can be used to study dynamic corrosion processes that

* Corresponding author. Netherlands Defence Academy, Faculty of Military Sciences, P.O. Box 10000, 1780CA, Den Helder, the Netherlands.
E-mail addresses: A.M.Homborg@tudelft.nl (A. Homborg), J.M.C.Mol@tudelft.nl (A. Mol), T.Tinga@mindef.nl (T. Tinga).

https://doi.org/10.1016/j.engappai.2024.108044
Received 2 November 2023; Received in revised form 13 December 2023; Accepted 3 February 2024
Available online 8 February 2024

change considerably over time, e.g. the identification of pitting corrosion and/or corrosion inhibition of stainless steel and aluminium alloys (Homborg et al., 2013b, 2014b), optionally in combination with in-situ optical techniques (Denissen et al., 2019, 2022; Homborg et al., 2022). Additionally, these can be applied for the identification of microbiologically influenced corrosion (Homborg et al., 2014c) and for the proper analysis of single and overlapping transients (Homborg et al., 2016). A transient is a relatively brief feature in the signal and can often be associated to the occurrence of localized corrosion such as pitting (Homborg et al., 2013b). Typically, transients in an EN signal generate local maxima in the energy distribution of a time-frequency spectrum. Transients can also be detected automatically, as published by the authors before (Homborg et al., 2013b, 2014b, 2018). The advantage of automatic transient detection and analysis is that it yields a faster and more objective study of the time-frequency information visible in the CWT or HHT spectrum; only the information that is associated with the occurrence of transients is analysed, whereas information in between these transients is neglected, while keeping the transient criteria constant. A useful method of quantifying local maxima that are associated with transients is called Modulus Maxima. MM describe the evolution of wavelet maxima over the different timescales. A wavelet is an oscillation of a limited time span. The wavelet transform describes the original EN signal using a linear combination of wavelets. By scaling and translation of these wavelets, the signal can be described at different timescales, or frequencies. The CWT spectrum visualizes the energy distribution of the signal over these different timescales (frequency axis) and time points (time axis). This can be particularly useful in case of process kinetics that change over time, or in other words, non-stationary signals (Cottis et al., 2015). Transients emerging from processes with specific kinetic characteristics generate a corresponding pattern of MM within a specific frequency range in the CWT spectrum. Within each transient only the dominant frequency information is taken into account (Homborg et al., 2018). The effectiveness of MM for the (manual) classification of corrosion processes was demonstrated by the authors in earlier work (Homborg et al., 2018). MM potentially increased the objectivity of the EN analysis by means of a well-defined selection of local maxima within each transient, which was in turn located by the transient analysis procedure. In earlier work, the CWT transient analysis protocol and the MM results proved to be sufficiently effective on their own (Homborg et al., 2013b, 2014b, 2018). However, these still required human interpretation of the dominant frequency components to determine the underlying corrosion phenomenon. The next step is to automatically verify the extent to which specific local frequency information within a transient is associated to a specific type of corrosion. This task can be performed by machine learning.

The use of machine learning has given important momentum to the classification of corrosion using EN (Hou et al., 2017; Alves et al., 2017, 2019; Ren et al., 2023; Sanchez-Amaya et al., 2005; Jian et al., 2013). The common approach is to teach a machine learning algorithm the values of specific features that are associated to certain types of corrosion, materials or environments. These features are collected in a feature vector. Hence, a feature vector consists of a specific selection of features that are considered as predictors, or as being indicative for the types of corrosion that are of interest (Hou et al., 2017; Alves et al., 2019). Such a feature vector may e.g. contain parameters like the noise resistance R_n or characteristic charge q or -frequency f_n (Ren et al., 2023). The former provides information about the barrier properties of a layer that may be present at the corroding surface. The latter two indicate the overall type of corrosion; localized corrosion e.g. shows a low f_n and a high q (Sanchez-Amaya et al., 2005). Additionally, wavelet parameters can be used in the feature vector, such as the discrete wavelet transform energy distribution over timescales (Alves et al., 2017, 2019; Jian et al., 2013). The exact machine learning method that is used in literature varies significantly. In some cases neural networks are applied, in others a different machine learning approach is used. Examples are so-called Back Propagation (BP) (Jian et al., 2013), Support Vector Machine (SVM) (Alves et al., 2017, 2019; Jian et al., 2013), Multi-Layer Perceptron (MLP) (Alves et al., 2017, 2019), k-nearest neighbour (KNN) (Ren et al., 2023), Decision tree (Ren et al., 2023), Random forest (Hou et al., 2017; Ren et al., 2023), Adaboost (Ren et al., 2023) and Linear Discriminant Analysis (LDA) (Hou et al., 2017). A different approach could be to use a so-called Physics-Informed Neural Network (PINN) (Cuomo et al., 2022). This is a type of neural network that takes into account the underlying physics of the problem in the form of Partial Differential Equations (PDEs), which implies that these are known for the chemo-physical process under investigation (Cuomo et al., 2022).

In this work, images of time-frequency transient characteristics and hence direct pictures of corrosion kinetics rather than a vector of parameters derived from the raw EN data, serve as training input for a convolutional neural network (CNN). No further specification of image features is made. A CNN is selected for this analysis, as it is known to be particularly suitable for image classification. This adaptive and flexible approach is denoted as deep learning, where the CNN autonomously finds features or classifiers in the images that are associated to a specific class (MathWorks). This transforms the interpretation of EPN transient information into an image classification problem, i.e. without a necessary preselection of parameters. Only the learning of classes is supervised; the CNN is trained using two sets of images, each set belonging to a different class, or type of pitting corrosion in this case. In this work, these classes represent the pitting processes of AISI304 or AA2024-T3, both immediately after immersion. The approach introduced here exploits the advantages of an objective image-recognition machine learning procedure while bypassing the largest classical disadvantage, which is the persistent lack of sufficient training data. A clever selection of multiple slices of time-frequency spectra serves as training images. Each slice is selected by our transient analysis method. The use of time-frequency spectra ensures that each slice, or image, still contains the full frequency range. This ensures that each image contains all relevant information about the underlying chemo-physical process kinetics. By this way, a limited number of measurement signals can provide a multitude of training images. Moreover, the final classification of a new measurement signal is also typically based on multiple transients, and hence, images. As a result, a small number of misclassifications of individual images is less likely to result in misclassification of the entire signal, which increases the robustness of the proposed approach. Furthermore, no pre-defined parameters are used. It should also be emphasized that contrary to existing work on machine learning for the study of EN, here the entire process from raw data to final classification is automated, without any intervention of the user. The entire process of time-frequency transient analysis, image data selection, production of images, deep learning and corrosion classification makes this data analysis procedure quite objective. Summarized, the most important contribution of the present work is to introduce a novel procedure that decreases the classical need for large amounts of raw data for training and validation purposes, while still achieving a satisfactory classification robustness. A relatively small number of individual signals thereby generates a multitude of input images that still contain all relevant kinetic information about the underlying chemo-physical process.

2. Material and methods

2.1. Experimental details

The experimental data used for training and classification in this work was collected from previous works. EPN data of pitting of AISI304 immersed in a 0.01M HCl solution was collected from previous work introducing Hilbert spectra as a novel time–frequency characterization method for EN data (Homborg et al., 2013a). A total of 10 datasets were used to obtain 240 individual transients of AISI304. EPN data of pitting of AA2024-T3 immersed in a 0.1M NaCl solution was collected from work where the authors introduced transient analysis using Hilbert spectra of EN data for the identification of corrosion inhibition

(Homborg et al., 2014b). In this case, 1 dataset served to provide already 246 individual transients, of which the last 6 were removed in order to obtain a similar number of transients for both materials, or in other words, to have equally sized classes. This prevents overfitting of the CNN on the largest dataset. From an experimental point of view, EPN is more straightforward than electrochemical current noise (ECN), since EPN only requires a single working electrode as compared to two working electrodes in the case of ECN (Homborg et al., 2014a). This allows the correlation between surface features and signal characteristics (Homborg et al., 2022). Moreover, ECN involves the risk of both working electrodes not remaining nominally identical over the course of the experiment (Lowe et al., 2003; Jamali and Mills, 2016). This can influence experimental results after long immersion times. EPN signals obtained immediately after immersion served as training and validation data. In order to further investigate the robustness of machine learning based on the fusion between CWT transient analysis and MM, its effectiveness to characterize the pitting process of AA2024-T3 between 9 and 10ks after immersion is investigated. This timeframe was considered as a suitable balance between a progressed pitting signal on the one hand and a still significant EPN signal amplitude for effective transient detection on the other hand. As the pitting process progresses over the course of the experiment, the working electrode surface slowly degrades further and the process kinetics and hence the transient frequency information also changes gradually. This complicates the automated classification for the machine learning procedure, which is only trained using the pitting characteristics of both materials up to 1ks after immersion with the formerly mentioned 11 (10 AISI304 and 1 AA2024-T3) datasets. For classification purposes, i.e. for testing the classification ability of the procedure, the pitting processes immediately after immersion of AISI304 and AA2024-T3 are represented by 3 EPN signals each. The remaining 3 EPN signals represent the pitting process of AA2024-T3 from 9 to 10ks after immersion. The sampling frequency of the AISI304 data was 5 Hz, whereas that of the AA2024-T3 raw data was 20 Hz. To eliminate any differences between the datasets, the AA2024-T3 data were therefore down sampled in MATLAB to 5 Hz. This resulted in equal frequency (y-) axes in the CWT spectra of both datasets. The EPN data were obtained with a Compactstat from Ivium Technologies, which was run by a Windows-based PC. The data were processed using MATLAB from Mathworks.

The basis of the transient analysis procedure is described elsewhere (Homborg et al., 2013b, 2014b, 2018). The analytic Morlet wavelet was applied for calculation of the CWT (Homborg et al., 2016). In essence, the transient analysis method applied in this paper identifies the locations of transients based on maxima present in the CWT spectrum at two separate frequencies: 1 Hz and 10^{-1} Hz. Local maxima in the CWT spectrum at either of both frequencies are designated as corresponding to a transient phenomenon occurring in the underlying process kinetics. For each transient location in time, the exact transient area in the CWT spectrum is defined as ranging from the time point where the absolute value of the EN signal becomes larger than the DC drift to where the absolute value of the EN signal again drops below the DC drift. In earlier work, a moving average smoothing filter was adopted for this task (Homborg et al., 2013b). In case no start and/or end point could be defined, a default timespan of 2 s is defined as transient duration. Even if the actual transient duration would be longer in this case, the time-frequency information is still expected to be captured within this timeframe of 2 s. However, a shorter timespan increases the risk of false double counts that in fact represent the same transient event. All time-frequency information in the area in between transient start and end in the CWT spectrum, including the MM, is then associated to a specific, individual transient phenomenon (Homborg et al., 2018). It should be noted here that consistency in the type of transient analysis procedure to be used for all datasets is considered to be more important than the exact type of transient analysis procedure. The authors consider the transient analysis procedure as an evolving element of the proposed data analysis procedure.

2.2. Data imaging and deep learning

After transient analysis, each area of interest in the CWT spectrum containing the time-frequency information of an individual transient is transformed into an individual PNG image using MATLAB. This results in a set of 240 AISI304 and 240 AA2024-T3 images, i.e. 480 images in total. Examples of this procedure are provided in the 'Results and Discussion' section. In order to achieve the deep learning classification of pitting corrosion, the CNN is trained using these images. In brief, a CNN consists of interconnected nodes or neurons in a layered structure. Each neuron is in fact a processing unit and so a CNN consists of layers of processing units that are interconnected: each neuron in a specific layer is connected to neurons of the next layer. Each layer of processing units performs a specific task in the process of image analysis and classification. These tasks include in a chronological order: (i) specification of the image size, which is 201 (time axis)-by-99 (frequency axis) pixels in this work, (ii) specification of the filter characteristics that are used in the training function, (iii) optimisation of the training process by normalizing gradients that may originate from transients in the data and which can propagate undesirably through the CNN, (iv) down-sampling, which is a process of reducing the number of data points in order to decrease the computation time per layer, (v) connecting the neurons to the neurons in the preceding layer in order to combine all the features learned by the previous layers across the image to identify larger patterns and (vi) normalization of the output and computation of the loss. The CNN used in this work is described in detail in (MathWorks), and among else comprises of three convolutional layers with 8, 16 and 32 filters, respectively, with a size of 3x3 pixels each. Changing any parameters in order to further optimise this CNN was outside the scope of the present work. Future work may incorporate a more optimised machine learning algorithm with possibly more layers, to capture finer transient details and to increase the CNN accuracy even further. Fig. 1 shows a flowchart of the process from the EPN measurement to final corrosion classification.

The separation into a training and validation set prior to the training process was necessary to verify the training success already at this stage. In this work, out of the 2x240 images generated from the 11 signals, 75% is used for training and 25% for validation. The classification data presented in the Results and Discussion section was not part of this data set, and was only offered to the CNN for the first time during the classification process.

3. Results and discussion

This section describes the results of automated corrosion classification by deep learning of the time-frequency information of EPN transients of pitting corrosion of AISI304 and AA2024-T3 based on 9 separate datasets. Additionally, this section discusses the effect of combining data from CWT transient analysis and MM on the classification accuracy. In this section, first the data analysis procedure will be explained based on one example data set of each material, AISI304 and AA2024-T3. Subsequently, training of the CNN is performed, using either only the CWT transients, only MM or the combined images of both. This resulted in three different trained versions of the same CNN. Finally, the classification accuracies of these three CNNs were compared for 6 individual datasets of AISI304 and AA2024-T3 immediately after immersion, as well as for 3 datasets of AA2024-T3 between 9 and 10ks after immersion.

Fig. 2 shows example micrographs of pitting corrosion of AISI304 and AA2024-T3 exposed to 0.01M HCl and 0.1M NaCl, respectively.

Fig. 2a shows an example of a corrosion pit of AISI304 exposed to 0.01M HCl for a duration of 1 ks, indicated by the white arrow. The pit depth is approximately 1 μm. Fig. 2b shows an example of corrosion pits of AA2024-T3 exposed to 0.1M NaCl for a duration of 14.5 ks? One of the pits is indicated by the white arrow. Pit depths are in the range of 2 μm. The corrosion attack of AA2024-T3 is notably more severe, as the

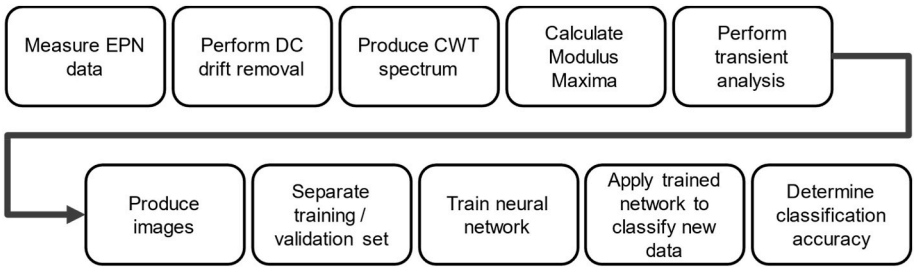

Fig. 1. Example flowchart of the machine learning process.

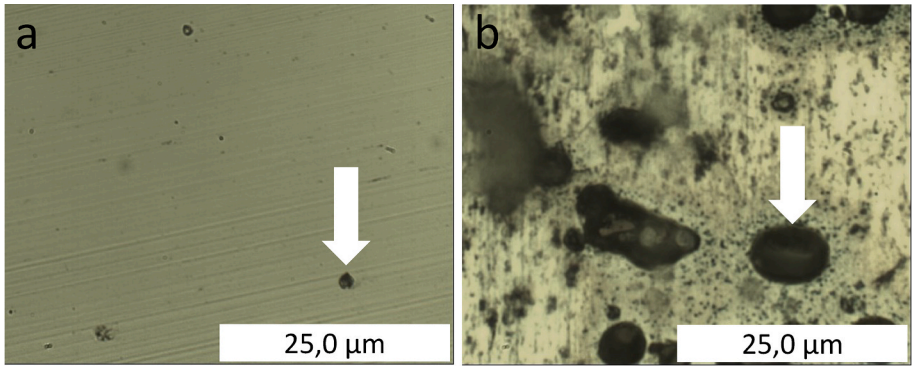

Fig. 2. (a) Micrograph of the surface of AISI304 exposed to 0.01M HCl for a duration of 1 ks and (b) Micrograph of the surface of AA2024-T3 exposed to 0.1M NaCl for a duration of 14.5 ks Corrosion pits indicated by the white arrows.

micrographs were produced after a longer exposure time and the intermetallic particles present in this alloy act as local cathodic sites from the start or after early stage dealloying (Homborg et al., 2014b; Kosari et al., 2020). Nevertheless, localized corrosion in general is very hard to detect or predict given its complex dynamic nature and dependence on time and spatially resolved heterogeneity of electrolyte and metallurgical characteristics, emphasizing the need for reliable monitoring and data classification.

In order to explain the data analysis protocol depicted in Figs. 1, Figs. 3–7 demonstrate the step-by-step procedure based on two example EPN signals from AISI304 and AA2024-T3. The first step in the data analysis procedure is to subtract the DC drift component from the raw EPN data (Homborg et al., 2012). Fig. 3a and b show the example EPN raw data sets of AISI304 and AA2024-T3 immersed in a 0.01M HCl and 0.1M NaCl solution, respectively, in black and their DC drift in grey (smooth line). Fig. 3c and d show their detrended signals, obtained by subtracting the grey trend from the black signal.

Fig. 3 indicates that the drift removal process, when executed correctly, maintains the transient information while removing the low-frequency DC drift. After DC drift removal, the EPN data is transformed into the time-frequency domain using CWT. MM can subsequently indicate the local maxima of transients, which can be a useful tool for the characterisation of the process kinetics (Homborg et al., 2018).

Fig. 4 shows the CWT spectra of the example EPN signals of (a) AISI304 and (b) AA2024-T3 that were shown in Fig. 3c and d, respectively. Fig. 4c and d show the MM in black. Fig. 4e and f show the same CWT spectra as in Fig. 4a and b with the MM as an overlay in black. In these CWT spectra, the x-axis represents time, the y-axis frequency and the z-axis (along with the corresponding colour scales) the instantaneous amplitude in (V).

The MM depicted in Fig. 4c and d indicate the locations in the signal with the highest singularity. Hence, MM follow the local maxima of the spectra shown in Fig. 4a and b from high to low frequency, which is visible in the combined information depicted in Fig. 4e and f: for some larger transients, the MM extend further down towards lower frequencies in the spectra. This can be useful information for the research of corrosion kinetics, however this requires a manual study of time-frequency spectra which can be quite time-consuming. The transient analysis-based CNN approach presented in this paper aims to provide a solution for this, with an automated classification including a quantified accuracy as output.

Fig. 5 shows the EPN signal of the two alloys after DC drift removal including their transient locations. These transient locations are

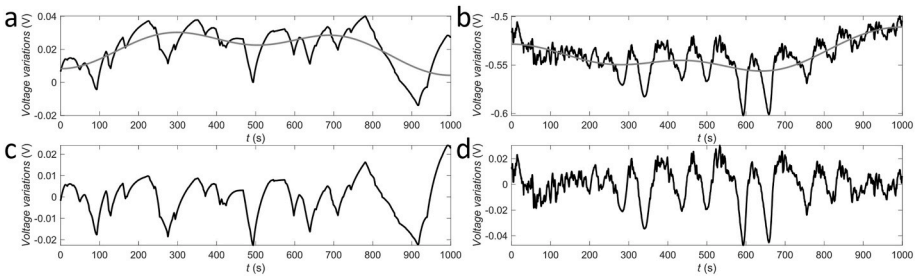

Fig. 3. Raw electrochemical potential noise data (black) including DC drift (grey, smooth line) of (a) AISI304 and (b) AA2024-T3 immersed in a 0.01M and 0.1M solution for a duration of 1 ks, respectively, and the detrended signals of (c) AISI304 and (d) AA2024-T3.

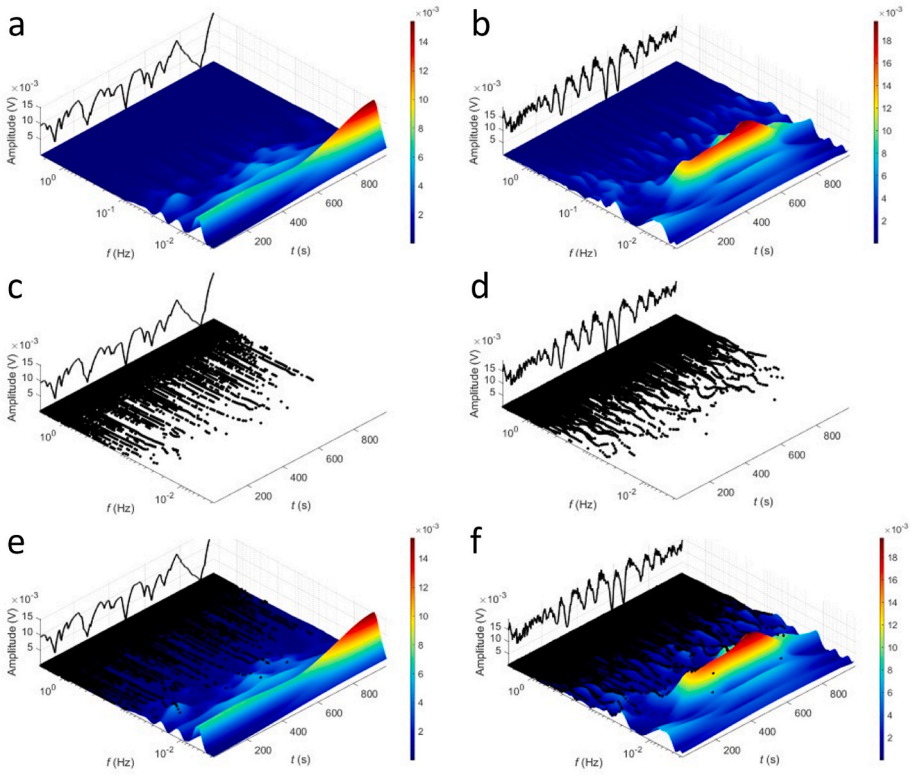

Fig. 4. (a, b) Continuous wavelet transform (CWT) spectrum, (c, d) only Modulus Maxima (MM) and (e, f) CWT spectrum with the MM as an overlay in black of the electrochemical potential noise signal after DC drift removal of AISI304 (Fig. 4 a, c, e) and AA2024-T3 (Fig. 4 b, d, f) immersed in a 0.01M HCl and 0.1M NaCl solution, respectively, for a duration of 1ks.

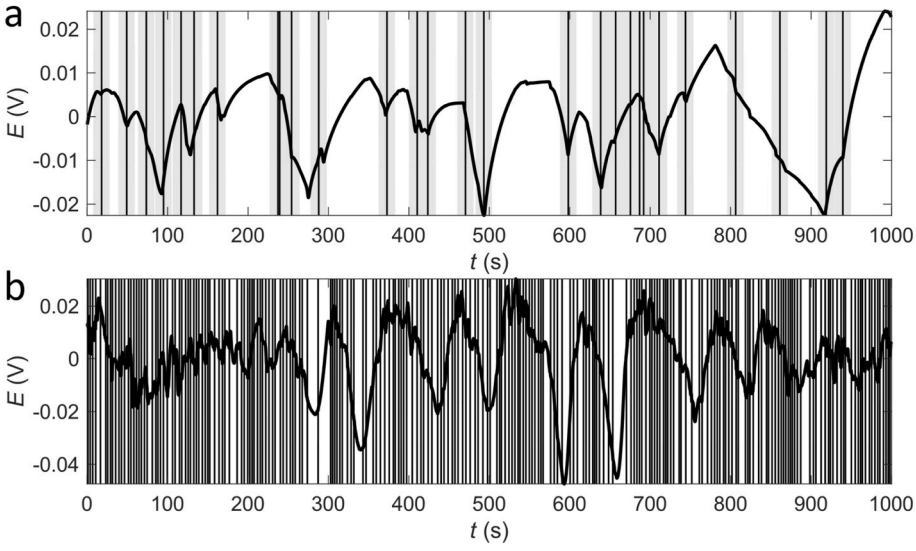

Fig. 5. Electrochemical potential noise (EPN) data including transient locations (black vertical lines) and estimated durations (grey areas) of the EPN signal after DC drift removal of (a) AISI304 and (b) AA2024-T3 immersed in a 0.01M HCl and 0.1M NaCl solution, respectively, for a duration of 1ks.

indicated by black vertical lines and their durations, in between transient start and end time, are indicated in grey.

The next step is to separate the CWT spectrum into smaller individual spectra, or 'slices', each representing one specific transient, i.e. from transient start to end. This is performed for three cases: for the CWT spectrum without MM, for only the MM as well as for the CWT spectrum including the MM as an overlay.

Each CWT spectrum is in fact a matrix with the columns representing the amplitudes of the frequencies that are composing the EPN signal at a specific time sample. Each time sample is therefore associated to one column in the matrix. From transient start to end, each individual transient is therefore also associated to a collection of columns in the matrix. For each transient individually, this leads to a smaller matrix that consists of this selection of columns. Subsequently, each of these smaller transient matrices is transformed into an image. In order to achieve this, the numbers in the matrices are represented as colours in a colour map. The range of the colour map corresponds to the total range of the numbers in the cells. This is comparable to the use of a colour map

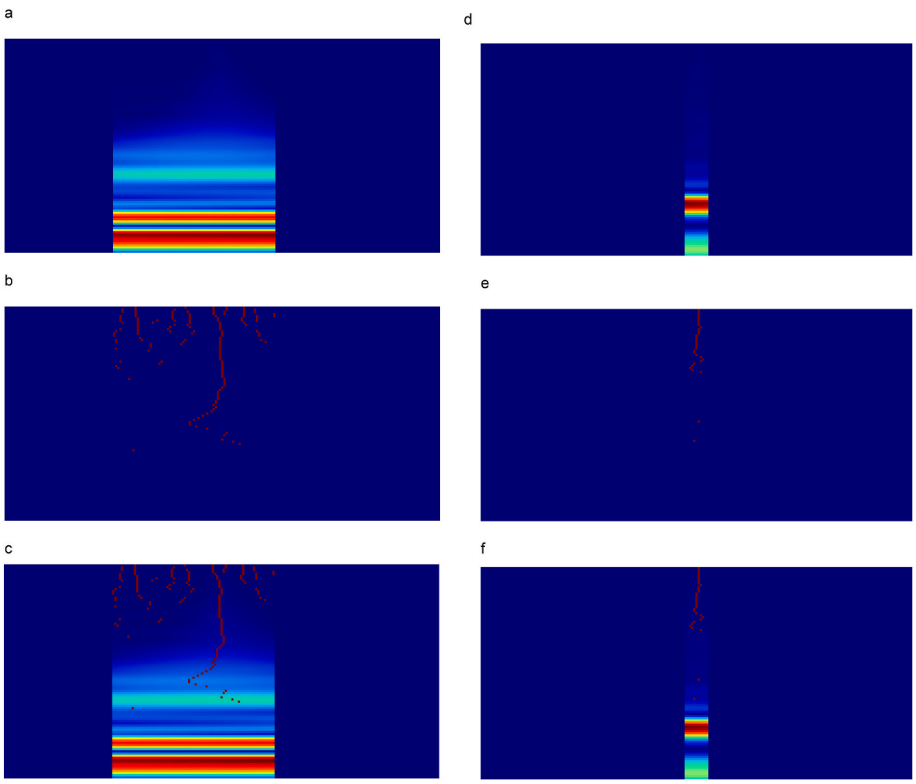

Fig. 6. Example of transient images of AISI304 including (a) only the continuous wavelet transform (CWT) spectrum, (b) only Modulus Maxima (MM) and (c) the CWT spectrum and MM, immersed in a 0.01M HCl solution for a duration of 1ks. Example of transient images of AA2024-T3 including (d) only the CWT spectrum, (e) only MM and (f) the CWT spectrum and MM, immersed in a 0.1M NaCl solution for a duration of 1ks.

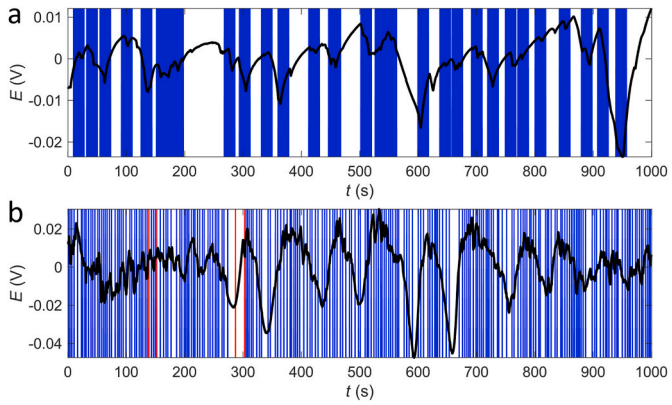

Fig. 7. Electrochemical potential noise data of AISI304 immersed in a 0.01M HCl solution (a) and of AA2024-T3 immersed in a 0.1M NaCl solution (b) for a duration of 1 ks, including transient locations and classification in colour code. Blue = correct classification (AISI304 in Fig. 7a and AA2024-T3 in Fig. 7b), red = incorrect classification.

for the visualization of the CWT spectra of Fig. 4. The MM, which are in fact matrices of zeros with ones only at the locations of the MM, are represented by the colour that corresponds to the maximum of the CWT spectrum. The zeros are left transparent in order to make the underlying CWT spectrum visible, similar to Fig. 4e and f. For each class (AISI304 and AA2024-T3) three types of images are produced: 1) only the CWT spectrum, 2) only MM or 3) the combined form of the CWT spectrum and MM. Fig. 6a–c show an example of these three types of images for AISI304 and Fig. 6d–f show an example of these three types of images for AA2024-T3. In Fig. 6b, c, e and f, the MM are the dark red squares, since dark red corresponds to the maximum of the chosen colourmap. As was noted in Fig. 5, the transient widths differ. The CNN however requires images of similar size. Therefore, all image sizes are adjusted to the width of the largest transient. This generates the dark blue parts at the left and at the right of most of the images, since dark blue corresponds to the minimum of the chosen colourmap. Moreover, the transient start and end point are not necessarily located symmetrically around the estimated transient location, which is always placed at the centre of each image.

The operation described above is performed for both training datasets; each of the 480 transients resulted in an image containing either 1) only the CWT spectrum, 2) only MM or 3) the CWT spectrum and MM. For each of these three options, the training images for each type of process, either pitting of AISI304 or AA2024-T3, were stored in two folders denoted as AISI304 and AA2024-T3. By this way, the CNN is trained using the correct data label (AISI304 or AA2024-T3) for each dataset. Firstly, it was trained with the AISI304 and AA2024-T3 folder containing images with only the CWT spectrum. This version of the CNN was stored. Then the same operation was repeated with the AISI304 and AA2024-T3 folders containing images with only MM and with the AISI304 and AA2024-T3 folders containing images with the CWT spectrum and MM. As a result, three versions of the trained CNN were available for classification: 1) CNN based on only the CWT spectrum, 2) CNN based on only MM and 3) CNN based on the CWT spectrum and MM.

The extraction of image features is unsupervised. As such, there is no pre-direction from the user to the CNN here, and the training process occurs fully flexible. After the training phase, the same operation is performed for the classification datasets. All transient images are stored in a classification folder and the trained CNN should classify the images using the previously trained features. This implies that each image, or transient, is classified as representing pitting of either AISI304 or AA2024-T3. This procedure decreases the risk of misclassification of an entire EPN signal, since an EPN signal often contains multiple transients that are all classified individually. Moreover, at a later stage this

procedure could provide a way to automatically detect changing corrosion parameters over time, by training different stages of a process as separate classes. The classification of the detrended EPN signals from Fig. 3c and d using the combination of the CWT spectrum and MM is visualized in Fig. 7. Fig. 7 is similar to Fig. 5, with the transient areas now coloured corresponding to the classification of each transient: blue = correct classification (AISI304 in Fig. 7a and AA2024-T3 in Fig. 7b), red = incorrect classification.

In Fig. 7 it is visible that although the classification process is not perfect, in this case all AISI304 transients are correctly classified as representing pitting of AISI304. The large majority of the transients of AA2024-T3 are classified correctly as well, as being pitting of AA2024-T3. Table 1 provides the number of counts per class for the AA2024-T3 signal of Fig. 7b, with a total of 228 transients in the entire signal.

Hence, the corrosion processes are correctly classified as pitting of AISI304 (Fig. 7a) and AA2024-T3 (Fig. 7b), with a classification accuracy of 224/228 = 0,98. This operation is performed for all 9 individual EPN datasets: 3 EPN signals from pitting of AISI304 from 0 to 1ks after immersion and 3 EPN signals from pitting of AA2024-T3 from both 0-1ks and 9-10ks after immersion. Table 2 provides the classification results. Classification accuracies below 0.75 are marked in bold face as being notably low. The average classification accuracies, together with their standard deviations, are displayed at the bottom of the table, also in bold face.

The classification accuracy of the proposed machine learning protocol of treating time-frequency transient information as an image-classification problem, is quite satisfactory at 0.97 when using CWT combined with MM. The classification accuracy of the CNN based on the two individual types of data is lower than that, with 0.72 (only CWT spectrum) and 0.84 (only MM). Hence, for the examples provided in this paper, the proposed method adds value for an accurate corrosion classification. However, it is necessary here to combine the CWT spectrum with MM. Additionally, the use of only MM results in a higher classification accuracy than the use of only the CWT spectrum. The authors hypothesize that this could be explained by the more discrete character of MM: either 1 or 0. The CWT spectrum is expected to exhibit a larger discrimination ability between local amplitudes, using the entire resolution of the applied colour map. Although this enables a greater ability to distinguish between the time-frequency characteristics of different transients, this could result in less pronounced differences between the two classes of transients. However, this may also be explained the other way around, with a larger discrimination ability between local amplitudes leading to an easier distinction between different classes of corrosion. Therefore, this remains merely an observation in the present work, that requires further study. Another observation in this respect is that for the AISI304 dataset #3 investigated here, exactly the opposite order of classification accuracy is the case, although with a small margin: the most accurate result is obtained by using only the CWT spectrum, after this only MM and the CWT spectrum combined with MM performs the worst. The differences are however very small. In fact, all three methods perform quite satisfactory with a minimum accuracy of 0.85. Therefore, no further conclusions are drawn here based on these subtle differences. More research on these aspects should provide more insight in this respect. In addition, it is interesting to observe that not only the average value of the classification accuracy based on the combined data is notably higher, but also no outliers in the classification accuracy below 0.75 exist. The number of outliers below 0.75 decreases from using only the CWT spectrum (4) to only MM (3, of which 0.73 is close to 0.75) to the combined data (0). This is in turn reflected in the standard deviation values, that decrease from only the CWT spectrum (0.28) to only MM (0.16) to the combined data (0.05). It should also be noted that a classification accuracy below 0.5 implies that the entire corrosion signal is misclassified. In the case of only the CWT spectrum, this is the case for 3 signals, all of which correspond to AA2024-T3. This leads to the final remark: in case of the use of only the CWT spectrum or MM, the CNN struggles with the classification of pitting of AA2024-T3 from 9 to 10ks after immersion. As the CNN is trained using datasets between 0 and 1ks after immersion, the more progressed form of this pitting process after 9ks of immersion is probably characterized by process kinetics that produce notable differences in the CWT spectrum and MM. This is particularly interesting, and would validate further research to quantify these differences in process kinetics. These should be investigated side by side with surface analysis data. However, after combining the CWT spectrum and MM, the CNN becomes more robust in its classification of also this more progressed form of pitting of AA2024-T3.

Table 1
Classification of the detrended AA2024-T3 electrochemical potential noise signal from Fig. 7b.

Class	# counts
AA2024-T3	224
AISI304	4

4. Conclusions

In this work, for the first time the time-frequency transient analysis of electrochemical potential noise (EPN) is treated as an image classification problem. Time-frequency spectral transient information of EPN signals obtained by continuous wavelet transform (CWT) could effectively be separated from the main spectrum and serve as input images for machine learning by a convolutional neural network (CNN). A small number of individual EPN signals thereby generated a multitude of input images, reducing the need for large amounts of input data while still obtaining satisfactory classification results. A layer of modulus maxima (MM) over the CWT spectra further increased the classification accuracy. Localised corrosion of AISI304 and AA2024-T3 immersed in a 0.01M HCl and 0.1M NaCl solution, respectively, could effectively be detected and classified. The average classification accuracy of the CNN based on the combined dataset of the CWT spectra with MM is higher (0.97, standard deviation 0.05) than based on the two individual types of data (0.72 for only the CWT spectra and 0.84 for only the MM, with standard deviations of 0.28 and 0.16, respectively). The more progressed form of pitting of AA2024-T3 after 9ks of immersion was also satisfactory classified by the machine learning procedure based on the combined dataset.

The procedure introduced in this work involves the creation of images that still contain all relevant kinetic information about the underlying chemo-physical process, while being derived from only a limited amount of raw data. By this, the classical need for large amounts of raw data is reduced with a still acceptable classification accuracy.

This paper serves as a proof of principle for the proposed method of image classification of time-frequency electrochemical potential noise transient information. Further research should indicate to what extent the amount of training data and type of CNN is important for the classification accuracy. This could entail a more optimised machine learning algorithm with possibly different filtering characteristics and more layers, to capture finer transient details and to increase the CNN accuracy even further. Additionally, future work should involve the characterisation of different localised corrosion processes. Examples of this would be the distinction of pitting and crevice corrosion of the same system, different stages of pitting, microbiologically influenced corrosion or the inhibition of, or re-activation of an inhibited corrosion process.

CRediT authorship contribution statement

Axel Homborg: Conceptualization, Data curation, Formal analysis, Investigation, Methodology, Validation, Visualization, Writing – original draft. **Arjan Mol:** Writing – review & editing, Validation. **Tiedo Tinga:** Writing – review & editing, Validation.

Table 2
Classification accuracy of 9 individual datasets of 1ks duration each. Classification accuracies below 0.75, as well as average classification accuracies and standard deviations, are marked in bold face.

Class	Timeframe	Classification accuracy only CWT spectrum	Classification accuracy only Modulus Maxima	Classification accuracy CWT spectrum & Modulus Maxima
AA2024-T3 #1	0-1ks	0.91	0.91	1.00
	9-10ks	**0.47**	**0.63**	0.96
AA2024-T3 #2	0-1ks	0.77	0.90	1.00
	9-10ks	**0.28**	**0.56**	0.96
AA2024-T3 #3	0-1ks	**0.47**	0.93	0.98
	9-10ks	**0.57**	**0.73**	0.96
AISI304 #1	0-1ks	1.00	1.00	1.00
AISI304 #2	0-1ks	1.00	1.00	1.00
AISI304 #3	0-1ks	1.00	0.90	0.85
Average classification accuracy		**0.72**	**0.84**	**0.97**
Standard deviation		**0.28**	**0.16**	**0.05**

Declaration of competing interest

The authors declare no competing interests.

Data availability

Data will be made available on request.

Acknowledgements

The Netherlands Defence Academy and Delft University of Technology are gratefully acknowledged for enabling this research and accommodating the research work.

References

Aballe, A., Bethencourt, M., Botana, F.J., Marcos, M., 1999a. Wavelet transform-based analysis for electrochemical noise. Electrochem. Commun. 1, 266–270. https://doi.org/10.1016/S1388-2481(99)00053-3.

Aballe, A., Bethencourt, M., Botana, F.J., Marcos, M., 1999b. Using wavelets transform in the analysis of electrochemical noise data. Electrochim. Acta 44, 4805–4816. https://doi.org/10.1016/S0013-4686(99)00222-4.

Aballe, A., Bethencourt, M., Botana, F.J., Marcos, M., Sánchez-Amaya, J.M., 2001. Use of wavelets to study electrochemical noise transients. Electrochim. Acta 46, 2353–2361. https://doi.org/10.1016/S0013-4686(01)00424-8.

Alves, L.M., Cotta, R.A., Ciarelli, P.M., 2017. Identification of types of corrosion through electrochemical noise using machine learning techniques. In: ICPRAM 2017 - Proc. 6th Int. Conf. Pattern Recognit. Appl. Methods. 2017-Janua, pp. 332–340. https://doi.org/10.5220/0006122403320340.

Alves, L.M., Cotta, R.A., Ciarelli, P.M., Salles, E.O.T., Côco, K.F., Samatelo, J.L.A., 2019. Identification of corrosive substances and types of corrosion through electrochemical noise using signal processing and machine learning. J. Control. Autom. Electr. Syst. 30, 16–26. https://doi.org/10.1007/s40313-018-00423-0.

Carmona-Hernandez, A., Contreras-Cuevas, A., Uruchurtu-Chavarin, J., Gonzalez-Rodriguez, J.G., Orozco-Cruz, R., Galván-Martínez, R., 2023. Electrochemical noise of SCC inhibition of a supermartensitic stainless steel in sour solution. ECS Trans. 110, 29–37. https://doi.org/10.1149/11001.0029ecst.

Cottis, R.A., 2000. Simulation of electrochemical noise due to metastable pitting. J. Corrosion Sci. Eng. 3, 1–9.

Cottis, R.A., Homborg, A.M., Mol, J.M.C., 2015. The relationship between spectral and wavelet techniques for noise analysis. Electrochim. Acta. https://doi.org/10.1016/j.electacta.2015.11.148.

Cuomo, S., Di Cola, V.S., Giampaolo, F., Rozza, G., Raissi, M., Piccialli, F., 2022. Scientific machine learning through physics–informed neural networks: where we are and what's next. J. Sci. Comput. 92, 1–62. https://doi.org/10.1007/s10915-022-01939-z.

Denissen, P.J., Homborg, A.M., Garcia, S.J., 2019. Interpreting electrochemical noise and monitoring local corrosion by means of highly resolved spatiotemporal real-time optics. J. Electrochem. Soc. 166, C3275–C3283. https://doi.org/10.1149/2.0341911jes.

Denissen, P.J., Homborg, A.M., Garcia, S.J., 2022. Requirements for corrosion inhibitor release from damaged primers for stable protection: a simulation and experimental approach using cerium loaded carriers. Surf. Coating. Technol. 430, 127966 https://doi.org/10.1016/j.surfcoat.2021.127966.

Hladky, K., Dawson, J.L., 1981. The measurement of localized corrosion using electrochemical noise. Corrosion Sci. 21, 317–322. https://doi.org/10.1016/0010-938X(81)90006-8.

Hladky, K., Dawson, J.L., 1982. The measurement of corrosion using electrochemical 1/f noise. Corrosion Sci. 22, 231–237. https://doi.org/10.1016/0010-938X(82)90107-X.

Homborg, A.M., Tinga, T., Zhang, X., Van Westing, E.P.M., Oonincx, P.J., De Wit, J.H.W., Mol, J.M.C., Homborg, A.M., Tinga, T., Zhang, X., van Westing, E.P.M., Oonincx, P.J., de Wit, J.H.W., Mol, J.M.C., 2012. Time-frequency methods for trend removal in electrochemical noise data. Electrochim. Acta 70, 199–209. https://doi.org/10.1016/j.electacta.2012.03.062.

Homborg, A.M., van Westing, E.P.M., Tinga, T., Zhang, X., Oonincx, P.J., Ferrari, G.M., de Wit, J.H.W., Mol, J.M.C., 2013a. Novel time–frequency characterization of electrochemical noise data in corrosion studies using Hilbert spectra. Corrosion Sci. 66, 97–110. https://doi.org/10.1016/j.corsci.2012.09.007.

Homborg, A.M., Tinga, T., Zhang, X., Van Westing, E.P.M., Oonincx, P.J., Ferrari, G.M., De Wit, J.H.W., Mol, J.M.C., 2013b. Transient analysis through Hilbert spectra of electrochemical noise signals for the identification of localized corrosion of stainless steel. Electrochim. Acta 104. https://doi.org/10.1016/j.electacta.2013.04.085.

Homborg, A.M., Tinga, T., Van Westing, E.P.M., Zhang, X., Ferrari, G.M., de Wit, J.H.W., Mol, J.M.C., 2014a. A critical appraisal of the interpretation of electrochemical noise for corrosion studies. Corrosion 70, 971–987. https://doi.org/10.5006/1277.

Homborg, A.M., Van Westing, E.P.M., Tinga, T., Ferrari, G.M., Zhang, X., De Wit, J.H.W., Mol, J.M.C., 2014b. Application of transient analysis using Hilbert spectra of electrochemical noise to the identification of corrosion inhibition. Electrochim. Acta 116. https://doi.org/10.1016/j.electacta.2013.11.084.

Homborg, A.M., Leon Morales, C.F., Tinga, T., De Wit, J.H.W., Mol, J.M.C., 2014c. Detection of microbiologically influenced corrosion by electrochemical noise transients. Electrochim. Acta 136. https://doi.org/10.1016/j.electacta.2014.05.102.

Homborg, A.M., Cottis, R.A., Mol, J.M.C., 2016. An integrated approach in the time, frequency and time-frequency domain for the identification of corrosion using electrochemical noise. Electrochim. Acta 222, 627–640. https://doi.org/10.1016/j.electacta.2016.11.018.

Homborg, A.M., Oonincx, P.J., Mol, J.M.C., 2018. Wavelet transform modulus maxima and holder exponents combined with transient detection for the differentiation of pitting corrosion using electrochemical noise. Corrosion 74, 1001–1010. https://doi.org/10.5006/2788.

Homborg, A.M., Olgiati, M., Denissen, P.J., Garcia, S.J., 2022. An integral non-intrusive electrochemical and in-situ optical technique for the study of the effectiveness of corrosion inhibition. Electrochim. Acta 403, 139619. https://doi.org/10.1016/j.electacta.2021.139619.

Hou, Y., Aldrich, C., Lepkova, K., Machuca, L.L., Kinsella, B., 2017. Analysis of electrochemical noise data by use of recurrence quantification analysis and machine learning methods. Electrochim. Acta 256, 337–347. https://doi.org/10.1016/j.electacta.2017.09.169.

Jamali, S.S., Mills, D.J., 2016. A critical review of electrochemical noise measurement as a tool for evaluation of organic coatings. Prog. Org. Coating 95, 26–37. https://doi.org/10.1016/j.porgcoat.2016.02.016.

Jian, L., Weikang, K., Jiangbo, S., Ke, W., Weikui, W., Weipu, Z., Zhoumo, Z., 2013. Determination of corrosion types from electrochemical noise by artificial neural networks. Int. J. Electrochem. Sci. 8, 2365–2377. https://doi.org/10.1016/S1452-3981(23)14315-X.

Kosari, A., Tichelaar, F., Visser, P., Zandbergen, H., Terryn, H., Mol, J.M.C., 2020. Dealloying-driven local corrosion by intermetallic constituent particles and dispersoids in aerospace aluminium alloys. Corrosion Sci. 177, 108947 https://doi.org/10.1016/j.corsci.2020.108947.

Lowe, A.M., Eren, H., Bailey, S.I., 2003. Electrochemical noise analysis: detection of electrode asymmetry. Corrosion Sci. 45, 941–955. https://doi.org/10.1016/S0010-938X(02)00179-8.

MathWorks, Create Simple Deep Learning Neural Network for Classification, (n.d.). https://nl.mathworks.com/help/deeplearning/ug/create-simple-deep-learning-network-for-classification.html (accessed November 1, 2023)..

Montoya-Rangel, M., Garza-Montes-de-Oca, N.F., Gaona-Tiburcio, C., Almeraya-Calderón, F., 2023. Corrosion mechanism of advanced high strength dual-phase steels by electrochemical noise analysis in chloride solutions. Mater. Today Commun. https://doi.org/10.1016/j.mtcomm.2023.105663.

Recio-Hernández, J.A., Landa-Gómez, A.E., Miguel, G.J.F.-S., Mejía-Sánchez, E., López-Huerta, F., Orozco-Cruz, R., Galván-Martínez, R., 2023. Electrochemical noise study of the passivation of AISI 1018 carbon steel as reinforcements embedded in ternary concretes during the setting process. ECS Trans. 110, 159–167. https://doi.org/10.1149/11001.0159ecst.

Ren, Z., Li, Q., Yang, X., Wang, J., 2023. A novel method for identifying corrosion types and transitions based on Adaboost and electrochemical noise. Anti-corrosion Methods & Mater. 2, 78–85. https://doi.org/10.1108/ACMM-11-2022-2725.

Rivera-cerezo, H., Gaona-tiburcio, C., Cabral-miramontes, J., Bautista-Margulis, R.G., Nieves-Mendoza, D., Maldonado-Bandala, E., Estupiñán-López, F., Almeraya-Calderón, F., 2023. Effect of heat treatment on the electrochemical behavior of AA2055 and AA2024 alloys for aeronautical applications. Metals 13, 1–24. https://doi.org/10.3390/met13020429.

Sanchez-Amaya, J.M., Cottis, R.A., Botana, F.J., 2005. Shot noise and statistical parameters for the estimation of corrosion mechanisms. Corrosion Sci. 47, 3280–3299. https://doi.org/10.1016/j.corsci.2005.05.047.

Xia, D.-H., Ji, Y., Zhang, R., Mao, Y., Behnamian, Y., Hu, W., Birbilis, N., 2023. On the localized corrosion of AA5083 in a simulated dynamic seawater/air interface—Part 1: corrosion initiation mechanism. Corrosion Sci. 213, 110985 https://doi.org/10.1016/j.corsci.2023.110985.